

# Momentum isotropisation in random potential

Thomas Plisson, Thomas Bourdel, Cord A. Mueller

# ▶ To cite this version:

Thomas Plisson, Thomas Bourdel, Cord A. Mueller. Momentum isotropisation in random potential. The European Physical Journal. Special Topics, 2013, 217, pp.79-84. hal-00814726

# HAL Id: hal-00814726

https://hal-iogs.archives-ouvertes.fr/hal-00814726

Submitted on 19 Apr 2013

HAL is a multi-disciplinary open access archive for the deposit and dissemination of scientific research documents, whether they are published or not. The documents may come from teaching and research institutions in France or abroad, or from public or private research centers. L'archive ouverte pluridisciplinaire **HAL**, est destinée au dépôt et à la diffusion de documents scientifiques de niveau recherche, publiés ou non, émanant des établissements d'enseignement et de recherche français ou étrangers, des laboratoires publics ou privés.

# Momentum isotropisation in random potentials

T.  $Plisson^1$ , T.  $Bourdel^1$ , and C. A.  $M\ddot{u}ller^{2,a}$ 

**Abstract.** When particles are multiply scattered by a random potential, their momentum distribution becomes isotropic on average. We study this quantum dynamics numerically and with a master equation. We show how to measure the elastic scattering time as well as characteristic isotropisation times, which permit to reconstruct the scattering phase function, even in rather strong disorder.

### 1 Introduction

These days, ultra-cold atoms permit to study disorder physics in a quantitative manner. In particular, quantum transport of non-interacting particles can be studied in 1D [1], 2D [2,3,4] and 3D [5,6]. One of the latest development, suggested in [7], consists in launching a quasi-monochromatic wave packet inside the bulk of a random potential and monitoring the single-particle momentum distribution [3,4]. The long-time evolution leads to coherent backscattering (CBS) and coherent forward scattering (CFS) signals, which are linked to weak and strong localization, respectively [8]. In this paper, we analytically and numerically analyze the short-time dynamics, which contains valuable information about disorder strength and scattering characteristics. In particular, we show how one can not only measure the scattering and transport times, but also reconstruct, by an angular Fourier analysis of the momentum distribution, the complete scattering phase function.

## 2 Momentum-distribution dynamics

Starting from the momentum distribution  $n_{\mathbf{k}}(0)$ , we seek to compute  $n_{\mathbf{k}}(t) = \overline{|\psi_{\mathbf{k}}(t)|^2}$  at later times t under the evolution with  $H = H_{\text{kin}} + V(\mathbf{r})$ . The over-bar  $\{.\}$  denotes an ensemble average over realizations of the random potential  $V(\mathbf{r})$ .

We simulate this evolution numerically by solving the two dimensional (2D) Schrödinger equation for matter waves with  $H_{\rm kin} = p^2/2m$  using a finite-difference method. The initial wave function has a small width  $\hbar \Delta k$  around a finite average momentum  $\hbar k_0$ . The random potential V(r) is an isotropic speckle with a Gaussian spatial covariance length  $\sigma$  and amplitude V. The natural energy and time scales of the system are  $E_{\sigma} = \hbar^2/m\sigma^2$  and  $t_{\sigma} = m\sigma^2/\hbar$ . Figure 1 shows numerically calculated momentum distributions, averaged over 1000 disorder realizations, for two different regimes:

<sup>&</sup>lt;sup>1</sup> Laboratoire Charles Fabry UMR 8501, Institut d'Optique, CNRS, Univ Paris Sud 11, 2 Avenue Augustin Fresnel, 91127 Palaiseau cedex, France

<sup>&</sup>lt;sup>2</sup> Centre for Quantum Technologies, National University of Singapore, 117543 Singapore

a e-mail: cord.mueller@nus.edu.sg

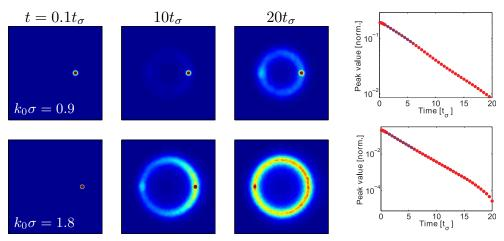


Fig. 1. Density plots of momentum distributions from the numerical simulation. Upper row: Experimental regime of [4], where  $k_0 = 0.9/\sigma$ ,  $V = 0.35E_{\sigma}$ , and  $\Delta k = 0.07k_0$ . Bottom row:  $k_0 = 1.8/\sigma$ ,  $V = 0.7E_{\sigma}$  and  $\Delta k = 0.035k_0$ . Parameters are chosen such that the weak-disorder ratio  $\Delta = 2V^2/(k_0\sigma)^2 \approx 0.3$  of perturbation theory is the same [9]. Right panels: the peak value  $n_{\mathbf{k}_0}$  of the initial momentum component decreases exponentially, Eq. (5). The indicated fits yield the elastic scattering times  $\gamma_0^{-1} = \tau_s = 6.7t_{\sigma}$  and  $2.4t_{\sigma}$ , respectively.

rather isotropic scattering with  $k_0\sigma = 0.9$  (upper row) and rather anisotropic scattering  $k_0\sigma = 1.8$  (bottom row).

As the initial peak at  $+\mathbf{k}_0$  decays, due to elastic scattering by the random potential, other momenta are populated on the (disorder-broadened) Rayleigh ring of radius  $k_0$ . Eventually, a CBS peak appears at  $-\mathbf{k}_0$ . In the remainder of this paper, we rather focus on the dynamics that produces the isotropic background.

From an analytical point of view, since unitary evolution conserves energy, it is appropriate to study the joint distribution  $n_{\mathbf{k}}(E,t)$  of energy and momentum, with marginal  $n_{\mathbf{k}}(t) = \int \frac{\mathrm{d}E}{2\pi} n_{\mathbf{k}}(E,t)$ . The density  $\psi\psi^*$  propagates according to

$$n_{\mathbf{k}}(E,t) = \int \frac{\mathrm{d}\omega}{2\pi} e^{-i\omega t} \sum_{\mathbf{k}'} \Phi_{\mathbf{k}\mathbf{k}'}(E,\omega) n_{\mathbf{k}'}(0), \tag{1}$$

where the intensity propagator  $\Phi_{kk'}(E,\omega)$  obeys the integral equation of motion [9,10]

$$[-i\omega + \gamma_{\mathbf{k}}(E)]\Phi_{\mathbf{k}\mathbf{k}'}(E,\omega) = A_{\mathbf{k}}(E)\left[\delta_{\mathbf{k}\mathbf{k}'} + \sum_{\mathbf{p}} U_{\mathbf{k}\mathbf{p}}(E,\omega)\Phi_{\mathbf{p}\mathbf{k}'}(E,\omega)\right]. \tag{2}$$

This form is valid for small frequencies  $\omega \ll E$  and can thus describe the dynamics at long enough times  $t \gg \hbar/E$ . The spectral function  $A_{\bf k}(E) = 2\pi \langle {\bf k} | \overline{\delta(E-H)} | {\bf k} \rangle$  is the probability density of a plane-wave state  ${\bf k}$  to have energy E. The vertex  $U_{{\bf k}{\bf p}}(E,\omega)$  describes all scattering events that couple  $\psi$  and  $\psi^*$ . It is related to the elastic scattering rate  $\gamma_{\bf k}(E)$  by the so-called Ward identity [9,11]

$$\gamma_{\mathbf{k}}(E) = \sum_{\mathbf{p}} A_{\mathbf{p}}(E) U_{\mathbf{p}\mathbf{k}}(E, 0). \tag{3}$$

This relation is a variant of the optical theorem, and expresses particle-number conservation. Using  $(-i\omega)\Phi_{kk'}(E,\omega)$  from (2) in (1) then yields the equation of motion

$$\partial_{t} n_{\mathbf{k}}(E, t) = A_{\mathbf{k}}(E) n_{\mathbf{k}}(0) \delta(t) - \gamma_{\mathbf{k}}(E) n_{\mathbf{k}}(E, t)$$

$$+ A_{\mathbf{k}}(E) \int \frac{\mathrm{d}\omega}{2\pi} e^{-i\omega t} \sum_{\mathbf{p}, \mathbf{k}'} U_{\mathbf{k}\mathbf{p}}(E, \omega) \Phi_{\mathbf{p}\mathbf{k}'}(E, \omega) n_{\mathbf{k}'}(0).$$

$$(4)$$

Initially, the populations at  $\mathbf{k}' \neq \mathbf{k}_0$  outside the initial wave packet are small. The most noteworthy evolution is the decay of  $n_{\mathbf{k}_0}$  as described by the first line of (4), whose solution immediately leads to  $n_{\mathbf{k}_0}(t) = \theta(t) \left[ \int \frac{\mathrm{d}E}{2\pi} A_{\mathbf{k}_0}(E) e^{-\gamma_{\mathbf{k}_0}(E)t} \right] n_{\mathbf{k}_0}(0)$ . This is a superposition of simple exponential decays, weighted by the spectral density. As function of E,  $A_{\mathbf{k}}(E)$  is rather sharply peaked around the effective excitation energy  $E_{\mathbf{k}}$ , whereas  $\gamma_{\mathbf{k}}(E)$  is smooth. Therefore, the dominant behaviour is

$$n_{\mathbf{k}_0}(t) = e^{-\gamma_0 t} n_{\mathbf{k}_0}(0) \tag{5}$$

with the elastic scattering rate  $\gamma_0 = \gamma_{\mathbf{k}_0}(E_{\mathbf{k}_0})$ .

The corresponding numerical data are shown in the right-hand panels of Fig. 1. For the two regimes of rather strong disorder studied here, we find  $\tau_s = 6.5t_{\sigma}$  for the first case and  $\tau_s = 2.4t_{\sigma}$  for the second. Lowest-order perturbation theory [9,12] overestimates the scattering strength and predicts  $\tau_s = 2.5t_{\sigma}$  and  $\tau_s = 1.4t_{\sigma}$ , respectively. We have, however, verified that if the simulation is run for  $V^2/EE_{\sigma} = 0.005 \ll 1$ , the measured value of  $\tau_s$  agrees with [9,12].

## 3 Diffusive isotropisation

#### 3.1 Master equation

Equation (4) describes the equilibration of populations due to potential scattering. Whenever the potential-scattering vertex  $U_{kk'}(E,\omega)$  is regular for  $\omega \to 0$ , the singular  $\omega$ -dependence of  $\Phi_{kk'}(E,\omega)$  dominates the  $\omega$ -integral. Using (1) and the Ward identity (3), one then arrives at a Markovian master equation of the Pauli type:

$$\partial_t n_{\mathbf{k}}(E, t) = \sum_{\mathbf{p}} U_{\mathbf{k}\mathbf{p}}(E) \left[ A_{\mathbf{k}}(E) n_{\mathbf{p}}(E, t) - A_{\mathbf{p}}(E) n_{\mathbf{k}}(E, t) \right]. \tag{6}$$

Assuming a factorised solution  $n_{\boldsymbol{k}}(E,t) = A_{\boldsymbol{k}}(E)n_{\boldsymbol{k}}(t)$ , we then obtain a closed master equation for the momentum distribution,  $\partial_t n_{\boldsymbol{k}}(t) = \sum_{\boldsymbol{p}} \bar{U}_{\boldsymbol{k}\boldsymbol{p}} \left[ n_{\boldsymbol{p}}(t) - n_{\boldsymbol{k}}(t) \right]$ , with transition rates  $\bar{U}_{\boldsymbol{k}\boldsymbol{p}} = \int \frac{\mathrm{d}E}{2\pi} A_{\boldsymbol{k}}(E) A_{\boldsymbol{p}}(E) U_{\boldsymbol{k}\boldsymbol{p}}(E)$ . The spectral functions fix the energies at  $E_{\boldsymbol{p}} \approx E_{\boldsymbol{k}}$ . Consequently, we can focus on the angular probability density  $n(\theta)$  on the circle  $\boldsymbol{k} = k_0(\cos\theta, \sin\theta)$  of elastic scattering. There, scattering from  $\theta$  to  $\theta'$  is described by the on-shell value  $U(\theta - \theta')$ . It is helpful to re-introduce the elastic scattering rate  $\gamma_0 = \nu_0 \int \mathrm{d}\theta U(\theta)$ , in accordance with (3);  $\nu_0 = \nu(E_{\boldsymbol{k}_0})$  denotes the

 $<sup>^1</sup>$   $U(\omega) \approx U(0)$  can only be factorised from the  $\omega$ -integral in (4) if it has no singular dependence in  $\omega$ . This is true at short times, since the single-scattering term does not depend on frequency at all and the frequency dependence is smooth for the first interference corrections. But the CBS contribution develops a diffusion pole at  $\omega=0$  and backscattering. Thus, the momentum distribution retains a memory of the initial condition and displays the CBS peak [7]. Even more singular terms appear at the onset of Anderson localisation and produce the CFS signal [8]. These phenomena are beyond the master-equation approach developed here.

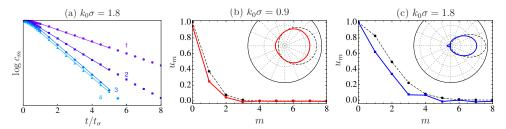


Fig. 2. (a) Fourier coefficients of the momentum distribution on the elastic scattering circle, up to m=4, as function of time, for the case  $k_0\sigma=1.8$ . Straight lines are fits to the exponential decay, Eq. (8), for  $t_\sigma < t < 5t_\sigma$ . (b) and (c) Fourier coefficients  $u_m$  of the scattering phase function, as measured from the numerical data (full red/blue), and at the single-scattering approximation, Eq. (9) (dashed black). The insets show the reconstructed phase functions, using moments up to m=4.

density of states. Finally, the elastic isotropisation of momentum is described by [see also Eq. (6.83) of [13]]

$$\partial_t n(\theta, t) = \gamma_0 \int_0^{2\pi} d\theta' u(\theta - \theta') \left[ n(\theta', t) - n(\theta, t) \right], \tag{7}$$

where  $u(\beta) = U(\beta) [\int d\theta U(\theta)]^{-1}$  is the normalised differential cross section of elastic scattering, the so-called phase function.

#### 3.2 Characteristic times

The convolution (7) on the unit circle can be readily solved by Fourier analysis: the coefficients  $c_m = \int d\theta e^{im\theta} n(\theta)$  obey the decoupled equations of motion

$$\partial_t c_m(t) = -\gamma_0 (1 - u_m) c_m(t) = -\tau_m^{-1} c_m(t) \tag{8}$$

in terms of the phase-function Fourier components  $u_m = \int \mathrm{d}\beta e^{im\beta}u(\beta)$ . By virtue of  $u_0 = 1$ , the zeroth mode  $c_0$  (i.e., the number of particles) is conserved. The first harmonic  $c_1$  decays exponentially on the transport-time scale  $\tau_1 = \tau_\mathrm{s}/[1-\langle\cos\beta\rangle]$ , with the usual notation  $\langle\cos\beta\rangle = u_1 = \int \mathrm{d}\beta\cos\beta u(\beta)$  [9]. Higher harmonics decay with their own times  $\tau_m = \tau_\mathrm{s}/[1-\langle\cos m\beta\rangle]$ .

Only for a completely isotropic phase function with  $\langle \cos m\beta \rangle = 0$  all times  $\tau_m$  are strictly identical to the elastic scattering time  $\tau_s$ . Things are more interesting for spatially correlated potentials. Indeed, at the single-scattering approximation, the Gaussian correlator  $U_{kp}^{(1)} \propto \exp\{-\sigma^2(k-p)^2/2\}$  has the phase function  $u^{(1)}(\beta) = \exp\{k^2\sigma^2\cos\beta\}/[2\pi I_0(k^2\sigma^2)]$  where  $I_0(\cdot)$  is the modified Bessel function. The corresponding Fourier coefficients

$$u_m^{(1)} = I_m(k^2\sigma^2)/I_0(k^2\sigma^2)$$
(9)

decrease as a function of the order m, such that the decay rates  $\tau_m^{-1}$  increase. In other words, the highest Fourier modes disappear first, giving way to an ever-broader background.

In Fig. 2(a), we show the time evolution of the first four Fourier coefficients  $c_m$  of the angular distribution in the case  $k_0\sigma = 1.8$ , as obtained from the numerical simulation data shown in Fig. 1 by a radial integration over a small interval around  $|\mathbf{k}| = k_0$ .

#### 3.3 Reconstruction of the phase function

From the measured decay of  $c_m(t)$ , one can compute the Fourier coefficients  $u_m$  via Eq. (8), and thus reconstruct the phase function  $u(\beta)$ . Fig. 2(b) and (c) show the  $u_m$  as measured from the numerical data, together with the single-scattering approximation (9). In the first case  $k_0\sigma = 0.9$ , the higher-order Fourier coefficients of the momentum distribution are very small. Consequently, the scattering phase function, shown in the inset of Fig. 2(b), is rather isotropic, as expected for  $k_0\sigma < 1$ . In the second case  $k_0\sigma = 1.8$ , the scattering is much more pronounced in the forward direction, as expected for  $k_0\sigma \gg 1$ .

Compared to the bare single-scattering phase functions (in dashed), the full reconstructed phase functions show a tendency towards enhanced backscattering. We may attribute this to weak localization corrections associated with short scattering paths, which are only known for isotropic scatterers [14].

### 4 Conclusion

We have analyzed the momentum isotropisation of a quasi-monochromatic wave packet inside a spatially correlated random potential. Results from the numerical calculation are well reproduced by a master-equation approach, even in regimes of strong disorder. We show how to reconstruct the phase function of elastic scattering from the measured exponential decay times of the angular components of the momentum distribution. This method is directly applicable in present-day experiments [3,4], and can serve as an *in situ* calibration of random potentials, for instance when investigating the impact of disorder in the presence of interactions [15,16].

**Acknowledgements:** T.P. is supported by IXBLUE. C.M. acknowledges financial support from Fondation des Sciences Mathématiques de Paris (FSMP) within the programme "Disordered Quantum Systems" at Institut Henri Poincaré. LCFIO is member of IFRAF and supported by CNRS, RTRA triangle de la physique, ANR-08-blan-0016-01, Isense. CQT is a Research Centre of Excellence funded by the Ministry of Education and the National Research Foundation of Singapore.

#### References

- 1. G. Roati et al., Nature 453, 895 (2008); J. Billy et al., Nature 453, 891 (2008).
- 2. M. Robert-de-Saint-Vincent et al., Phys. Rev. Lett. 104, 2 (2010).
- 3. G. Labeyrie, T. Karpiuk, B. Grémaud, C. Miniatura, D. Delande, arXiv:1206.0845.
- 4. F. Jendrzejewski et al., arxiv:1207.4775.
- 5. S.S. Kondov, W.R. McGehee, J.J. Zirbel, B. DeMarco, Science 334, 66 (2011).
- 6. F. Jendrzejewski et al., Nature Phys. 8, 398 (2012).
- 7. N. Cherroret et al., Phys. Rev. A 85, 011604(R) (2012).
- 8. T. Karpiuk *et al.*, arXiv:1204.3451.
- 9. R. C. Kuhn et al., Phys. Rev. Lett. 95, 250403 (2005) and New J. Phys. 9, 161 (2007).
- 10. E. Akkermans and G. Montambaux, Mesoscopic Physics of Electrons and Photons (Cambridge University Press, 2007).
- 11. D. Vollhardt and P. Wölfle, Phys. Rev. B 22, 4666 (1980).
- 12. M. Hartung et al., Phys. Rev. Lett. 101, 020603 (2008).
- 13. C. A. Müller, "Diffusive spin transport", Lect. Notes Phys. 768, 277-314 (2009).
- 14. F. Eckert, T. Wellens, A. Buchleitner, arXiv:1101.0995.
- 15. B. Allard et al., Phys. Rev. A 85, 033602 (2012).
- 16. M.C. Beller, M.E.W. Reed, T. Hong, S.L. Rolston, New J. Phys. 14, 073024 (2012).